ELSEVIER

(U–Th)/He ages of phosphates from St. Séverin LL6 chondrite

Kyoungwon Min [a,*], Peter W. Reiners [b], David L. Shuster [c,d]

[a] *Department of Geological Sciences, University of Florida, Gainesville, FL 32611, United States*
[b] *Department of Geosciences, University of Arizona, Tucson, AZ 85721, United States*
[c] *Department of Earth and Planetary Science, University of California, Berkeley, CA 94720, United States*
[d] *Berkeley Geochronology Center, 2455 Ridge Road, Berkeley, CA 94709, United States*

Abstract

We obtained single-grain (U–Th)/He ages from 14 merrillite and five chlorapatite aggregates from St. Séverin to constrain its low-T thermal history. In addition, we performed ^{3}He/^{4}He stepped heating diffusion experiments for merrillite and chlorapatite crystals from Guareña chondrite to better constrain He diffusion properties in chondritic phosphates in general. Among the 19 phosphate grains from St. Séverin, the five oldest merrillites and four oldest chlorapatites yielded weighted mean ages of 4412 ± 75 Ma (1σ: MSWD = 0.34) and 4152 ± 70 Ma (MSWD = 0.48), respectively. These weighted mean ages overlap with the peaks of the corresponding probability density plots, thus likely represent the most pristine (U–Th)/He ages of St. Séverin. The radiogenic ^{4}He and proton-induced ^{3}He diffusion experiments on Guareña chondrite resulted in two well-defined linear trends in Arrhenius plot for merrillite (radius = $\sim$59 μm) and chlorapatite ($\sim$43 μm) grains. Error-weighted linear regressions of the ^{3}He data yielded following diffusion parameters: $E_a = 135.8 \pm 4.8$ kJ/mol, and $\ln(D_o/a^2) = 5.83 \pm 0.66 \ln(\text{s}^{-1})$ for merrillite; and $E_a = 109.3 \pm 9.7$ kJ/mol, and $\ln(D_o/a^2) = 8.15 \pm 1.93 \ln(\text{s}^{-1})$ for chlorapatite. Assuming the analyzed fragments approximate the diffusion domain, $\log D_o$ was calculated as $(-1.93 \pm 0.29) \log(\text{cm}^2/\text{s})$ and $(-1.19 \pm 0.84) \log(\text{cm}^2/\text{s})$ for merrillite and chlorapatite, respectively. These results indicate higher closure T for merrillite than chlorapatite. Assuming these results also apply to St. Séverin and that crystal dimensions define the limiting diffusive length-scale, the closure temperatures of merrillite and chlorapatite in St. Séverin are estimated to be 94–112 °C (for cooling rates of 0.3–2.6 °C/Ma) and 18 °C (for 0.3 °C/Ma), respectively. The new single-grain (U–Th)/He ages and ^{3}He/^{4}He stepped heating diffusion results, combined with previously reported Pb/Pb and ^{40}Ar/^{39}Ar (with updated λ–t_{FCs} pairs) data indicate that St. Séverin experienced relatively rapid cooling from 477 °C down to $\sim$100 °C at a cooling rate of 2.6 °C/Ma. The identified thermal history is generally consistent with the reported cooling path from Pu fission track data. These results suggest that St. Séverin experienced relatively slow cooling compared to H chondrites, which may have resulted from its parent body size being larger than that of the H chondrites.
© 2012 Elsevier Ltd. All rights reserved.

1. INTRODUCTION

Thermal histories of meteorites provide key information regarding accretion processes, internal structures and physical dimensions of their parent bodies. An inverse relationship between cooling rate and metamorphic grade was identified for H chondrites, suggesting their parent body had a layered internal structure (Pellas and Storzer, 1981). This hypothetical internal structure, termed an "Onion Shell" model, was further supported by Pb/Pb (Göpel et al., 1994), ^{244}Pu fission track and ^{40}Ar/^{39}Ar data (Trieloff et al., 2003). From the detailed Pb/Pb isotopic data, Amelin et al. (2005) compared six different accretion scenarios (Ghosh et al., 2003), the most preferable of which proposes that accretion initiated 1.7 Myr after formation of the CAI (Calcium–Aluminum-rich Inclusion), then was followed by continuous growth during the next 3.6 Myr. A similar

approach was employed by Bouvier et al. (2007), who obtained high quality Pb isotopic data and modeled thermal histories of H, L, LL and CV parent bodies. The L and LL chondrites are believed to have experienced more prolonged cooling than the H chondrites (Pellas and Storzer, 1981; Bouvier et al., 2007), although a detailed variation of the cooling rate in relation to the metamorphic grade is yet to be established. Based on the differences in the cooling rates, it is often conjectured that the parent body of LL chondrites is larger than the H body (Pellas and Storzer, 1981; Bouvier et al., 2007).

Another important application of thermochronology to meteorites is to characterize the nature of impact-related dynamic processes that have occurred in their parent bodies. In the case of L chondrites, whole-rock $^{40}Ar/^{39}Ar$ and (U–Th)/He ages are concentrated near ~400–500 Ma (Heymann, 1967; Bogard et al., 1976; Wasson and Wang, 1991; Bogard, 1995; Korochantseva et al., 2007), which are commonly attributed to the parent bodies having experienced an intensive dynamic disruption during that period of time. In addition, the fossil meteorite fragments discovered in the mid-Ordovician (470 Ma) layers in Sweden (Schmitz et al., 1996) are confirmed to be L chondrites (Schmitz et al., 2001; Heck et al., 2004, 2008; Greenwood et al., 2007), suggesting that the thermochronologic data resetting was associated with intense bombardment and breakup of the parent bodies. Other examples of dynamic processes can be found for Martian meteorites, most of which experienced relatively intense shock metamorphism during their ejection from Mars. The thermochronologic constraints (Weiss et al., 2002; Min et al., 2004; Shuster and Weiss, 2005; Min and Reiners, 2007; Cassata et al., 2010) and conditions of peak metamorphism (Fritz et al., 2005) combined with other lines of evidence (such as cosmic-ray exposure ages) provide important clues regarding the timing and intensity of the ejection-related dynamic processes.

One primary goal of this study is to test if single-grain (U–Th)/He dating, which is routinely used for terrestrial samples, can be applied to chondritic meteorites. In contrast to terrestrial samples, meteoritic minerals present challenges in applying this method. First, the He diffusion properties in merrillite, the major U–Th bearing mineral phase in various types of meteorites including chondrites and Martian meteorites, are not characterized. For meteoritic apatite, the He diffusion properties were documented using Acapulco chlorapatite (Min et al., 2003), which yielded slightly higher closure temperatures than those of terrestrial Durango fluorapatite. However, there are no He diffusion experiments for merrillites, hampering thermochronologic interpretation of merrillite (U–Th)/He ages. Previous single-grain studies for Martian meteorites assumed that the He diffusion in merrillite is almost identical to that in apatite (Min et al., 2004; Min and Reiners, 2007). However, this assumption is poorly justified and requires more reliable characterization regarding He diffusion in merrillite.

Second, it is difficult to apply alpha (α) recoil correction to single-grains from meteorites. Because the phosphate grains in meteorites are very irregularly-shaped, with inter-

nal fractures in many cases, it is rarely possible to retrieve whole phosphate grains without any physical damage. Also, the available quantities of meteorite samples are typically very small compared to terrestrial samples, which seriously limits our capability to screen a large number of grains to find ideal ones. In previous studies, it was claimed that α-recoil correction is unnecessary for at least a few grains in Acapulco (Min et al., 2003) because the α-recoil-uncorrected ages (~4538 ± 32 Ma[1]) are old enough to be consistent with other thermochronologic data (e.g., $^{40}Ar/^{39}Ar$ and Sm/Nd). For the shocked Los Angeles Martian meteorite, it was also shown that α-recoil correction is unnecessary because the α-recoil-uncorrected ages are essentially identical to the cosmic-ray exposure ages within their uncertainties (Min et al., 2004). To explain the reason why they do not require α-recoil correction, Min (2005) suggested possible scenarios that may have occurred for selected grains during sample preparation. In this paper, we aim to test such hypothetical arguments regarding the sample preparation procedures.

The other major motivation of this research is to constrain the low-T (<200 °C) cooling history of St. Séverin LL6 chondrite using single-grain (U–Th)/He methods. The higher-T thermal history of St. Séverin is relatively well understood from U–Pb (Manhès et al., 1978; Göpel et al., 1994; Bouvier et al., 2007), K/Ar (Schultz and Singer, 1976) and $^{40}Ar/^{39}Ar$ (Hohenberg et al., 1981) isotopic systems. The low-T thermal history is documented from ^{244}Pu fission tracks in merrillite and attached phases (Pellas and Storzer, 1977, 1981). From these studies, it is generally agreed that St. Séverin cooled more slowly compared to H chondrites. Although there are some whole-rock (U–Th)/He data, the interpretations of these data were limited due to the possibility of He degassing during late-stage thermal events after primary metamorphism in the parent body. Because the low-T cooling history of St. Séverin is exclusively from the ^{244}Pu fission track data, which give cooling rates instead of absolute ages, our new (U–Th)/He data can provide important clues about the thermal history for temperatures below ~200 °C.

Schultz and Singer (1976) estimated the whole-rock (U–Th)/He age of 3.60 ± 0.45 Ga based on measured He concentrations combined with the previously reported U concentration of 12 ± 1 ppb and U/Th value of 3.6. They interpreted that mild thermal metamorphism caused diffusive loss of He, yielding whole-rock (U–Th)/He ages significantly younger than the K–Ar ages of ~4.40 Ga. Wasson and Wang (1991) compiled all the available U–Th–He data and calculated whole-rock (U–Th)/He ages for numerous ordinary chondrites. According to this compilation, the H and LL chondrite groups broadly define peaks in the range of 3–4 Ga, and St. Séverin's age was estimated to be 3.78 ± 0.51 Ga (error calculated from the cited value of 12–15%), which is consistent with the previous estimate of 3.60 ± 0.45 Ga. In this study, we attempt to test whether we can date initial cooling of parent bodies and minimize any complicating effects of potential late-stage thermal

---

[1] All uncertainties are given at 68% confidence or one standard deviation, unless otherwise specified.

event through single-grain phosphate (U–Th)/He dating of the St. Séverin meteorite.

In summary, the general goals of this research are (1) deducing general He diffusion properties in merrillite and apatite, which are the major reservoirs of U–Th in most meteorites, (2) testing if the complicated α-recoil correction procedures for meteorites can be avoided by choosing appropriate samples, and (3) constraining low-T thermal history of St. Séverin LL6 chondrite from single-grain (U–Th)/He dating. For these goals, we performed ^{3}He/^{4}He stepped heating experiments for merrillite and chlorapatite grains from Guareña chondrite, and single-grain (U–Th)/ He dating for phosphate aggregates from St. Séverin.

2. ANALYTICAL PROCEDURES

2.1. (U–Th)/He ages of St. Séverin

Approximately 1.7 g of St. Séverin chip was crushed and sieved. The extracted fragments, corresponding to 125–297 μm (mesh number of 120–50), were selected for this research because we intended to use large phosphate grains. According to the recent work of Jones and Dreeland (2010), 70% of the chlorapatite grains they identified in two thin sections of St. Séverin were smaller than 50 μm, and the remaining 30% were in the range of 90 μm to 150 μm. Also, these authors found that 60% of merrillite grains were <50 μm across, and the remaining 40% ranged from 50 to 275 μm. Therefore, the selected size fractions are expected to be larger than most of the phosphate grains in St. Séverin. The fragments were randomly spread on a carbon sticky tape, and chemically scanned using a scanning electron microscope (SEM). Based on elemental distributions of P, Ca, Si and Mg, we identified phosphate-bearing grains from grains of other minerals such as olivine, plagioclase, pyroxene, chromite, metal and sulfide. In all cases, the identified phosphates have other phases attached, and it was almost impossible to remove the attached phases without damaging the phosphates. The phosphates with the attached phases, which are called "phosphate aggregates" (Fig. 1), were used for our (U–Th)/He age determination. A total of 19 phosphate aggregates were used for chemical and (U–Th)/He analysis. Once the phosphate aggregates were identified, we examined them individually with a SEM at higher resolution to attain detailed chemical mapping and textural analysis (Fig. 1). To achieve semi-quantitative chemical compositions of the target phosphates, at least one area of the individual phosphates was analyzed using Energy Dispersive Spectroscopy (EDS). Because of the nature of our samples (unpolished, no artificial coating with conductive materials) and the limitation of the EDS methods, the accuracy of the determined chemical compositions is relatively poor.

The merrillite in St. Séverin has compositions close to the ideal formula (Na$_2$(Mg, Fe^{2+})$_2$Ca$_{18}$(PO$_4$)$_{14}$), with concentrations of MgO (~3.5 wt.%), Na$_2$O (~2.9 wt.%) and Cl (below detection limit). These are comparable to the merrillite compositions of MgO (0.91–3.5 wt.%) and Na$_2$O (0.7–2.5 wt.%) reported for four martian meteorites and one pallasite (Joliff et al., 2006). This is clearly distinct
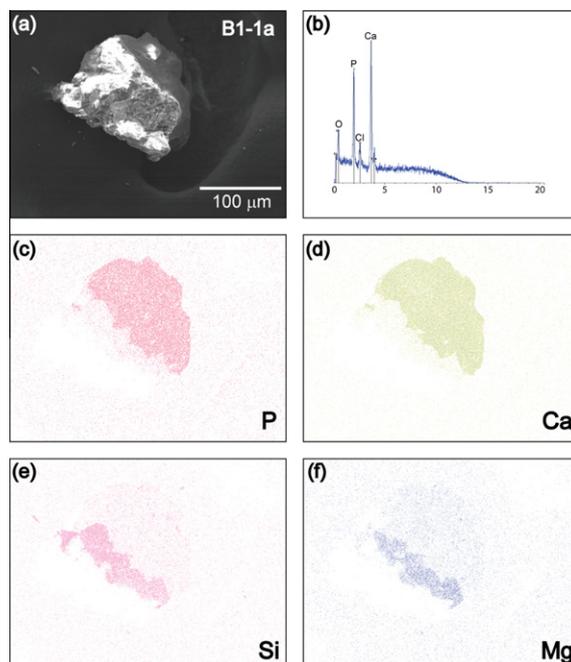

Fig. 1. SEM results obtained from the B1-1a phosphate aggregate sample, which was later used for (U–Th)/He age determination (4.02 ± 0.14 Ga). (a) Secondary electron image showing the shape of the sample. (b) EDS (Energy Dispersive Spectroscopy) results obtained from a circular spot on the phosphorous-rich area. The high Cl content and lack of Mg and Na indicate that the chemical composition of this phosphate corresponds to chlorapatite. (c∼f) Chemical maps for four elements used to identify the morphological relationships between phosphate and other phases. In this sample, more than ∼70% of the exposed surface corresponds to phosphate (chlorapatite) and the remaining <30% is Mg-rich silicate (orthopyroxene or olivine). Most of the phosphate aggregates used for this study have other phases attached. Each of the phosphate aggregates was examined under SEM to obtain such basic chemical and morphological data before destructive (U–Th)/ He analysis.

from the co-existing chlorapatite (MgO, below detection limit; Na$_2$O = 0.28 ± 0.02 wt.%; Cl = 4.3–5.4 wt.%) (Jones and Dreeland, 2010). Based on these chemical features, the selected 19 phosphates were identified as 14 merrillites and 5 chlorapatites. The high abundance of merrillite over chlorapatite in St. Séverin was also observed in a few thin sections (Crozaz, 1974; Jones and Dreeland, 2010). After the SEM analysis, the phosphate aggregates were carefully retrieved from the carbon sticky tape, and their physical dimensions were measured under a stereo microscope. Then, each grain was wrapped with a niobium tube, degassed with a Nd-YAG laser and its ^{4}He abundance was determined using a quadrupole mass spectrometer. To ensure complete He extraction from the samples, we performed multiple degassing experiments until the last step yielded less than 0.5% of the total ^{4}He. The sample packet was retrieved from the He line, mixed with U–Th–Sm spike, dissolved with strong acids (HF, HNO3), and the U, Th and Sm analysis was performed using Elemet2 ICP-MS. Details of the analytical procedures are available in Min et al. (2004).

The cosmogenic ^{4}He in each phosphate aggregate was calculated based on the following simple equation: ^{4}He$_{cos}$ = ^{4}He$_{cos}$ production rate [cc/g-Ma] × sample weight [g] × exposure age [Ma]. The ^{4}He$_{cos}$ production rate of 8.05×10^{-8} cc/g-Myr was estimated for chondrites (Eugster, 1988) based on the ^{3}He$_{cos}$ production rate (1.61×10^{-8} cc/g-Myr) and the relationship between ^{3}He$_{cos}$ and ^{4}He$_{cos}$ (Heymann, 1967; summarized in Min, 2005). The weight of each grain was estimated from the morphology and approximate density of the grain. However, because of the large uncertainties in these estimates, the errors of the calculated sample weight can be as large as ~30%. A range of exposure ages are estimated for St. Séverin based on Kr isotopes (13.0 ± 1.4 Ma: Marti et al., 1969), Ne isotopes (10.8 ± 0.2 Ma; Schultz and Singer, 1976) and Mn isotopes (10–14 Ma; Englert and Herr, 1978). To constrain the shielding effects of Kr isotopes in St. Séverin, Lavielle and Marti (1988) calculated an exposure age of 16.5 ± 1.8 Ma from the updated Ne calibration (Nishiizumi et al., 1980) and isotopic data (Schultz and Kruse, 1983). From this new estimate and their existing Kr exposure ages (Marti et al., 1969), Lavielle and Marti (1988) adopted the most likely exposure age of 14.8 ± 2.4 Ma, and this value is used for our ^{4}He$_{cos}$ calculation. The estimated ^{4}He$_{cos}$ to the total ^{4}He is generally less than 1% for samples older than 3 Ga (Table 1), but two samples yield rather high values (4.7% for SA1-9a; 3.0% for SA2-3a), drawing an attention to the ^{4}He$_{cos}$ correction procedures. The high ^{4}He$_{cos}$ to ^{4}He$_{total}$ ratios from these two aggregate samples likely result from their phosphate portions being small, thus yielding less ^{4}He$_{rad}$, in comparison with their hosting aggregate bodies.

We also calculated the ^{4}He contribution from now-extinct ^{244}Pu (half-life = 82 Ma), which can be important for phosphate grains in meteorites older than ~4.4 Ga

(Min, 2005). The existence of ^{244}Pu in St. Séverin is evidenced by ^{244}Pu-derived fission tracks (Cantelaube et al., 1967) and excess neutron-rich Xe isotopes (Wasserburg et al., 1969) in merrillites, but a precise quantitative estimate for ^{244}Pu is challenging. Although it is controversial, the ^{244}Pu/^{238}U values of 0.001–0.017 were suggested for various chondrites (Podosek, 1970; Hagee et al., 1990), and similar values were reported for apatites (0.004) and merrillites (0.011) in the Acapulco meteorite (Pellas et al., 1997). For merrillite in St. Séverin, an initial ^{244}Pu/^{238}U value of 1/30 (= 0.033) was suggested based on the assumption that ^{244}Pu was enriched with respect to U (Wasserburg et al., 1969). This value was, however, later revised to 0.012 with updated U–Th contents in merrillites combined with an assumption that ^{244}Pu was enriched with respect to Th (Crozaz, 1974). Because the Th/U value in apatite (2.7 ± 3.5) is lower than in merrillite (7.4 ± 5.0), as described in the following section, ^{244}Pu content during the early formation of St. Séverin is expected to be lower in apatite. Following the logic of Crozaz (1974), we calculated the ^{244}Pu/^{238}U in apatite as ~0.004 (= 0.012 × 2.7/ 7.4). Using these estimated ^{244}Pu/^{238}U values for merrillite (0.012: Crozaz, 1974) and apatite (0.004), the ^{244}Pu-induced ^{4}He content was calculated for the samples with ages older than 4 Ga (Table 1). The average contribution of this component to the total ^{4}He is ~0.23%, and the correction using individual contributions was incorporated for the final (U– Th)/He age calculations.

2.2. Helium diffusion experiments on meteoritic phosphates

To quantify the kinetics of He diffusion in meteoritic phosphate, we conducted stepwise degassing experiments on natural phosphates that were irradiated with energetic protons to ensure a uniform spatial distribution of ^{3}He

Table 1
(U–Th)/He data for phosphates in St. Séverin chondriteite.

Sample Name	U (pg)	Th (pg)	Sm (pg)	Th/ U	Sm/ U	^{4}He total (fmol)	^{4}He$_{cos}$ (%)	^{4}He$_{244Pu}$ (%)	^{4}He$_{147Sm}$ (%)	(U–Th)/He age (Ma)	1σ (Ma)	1σ (%)	Sm contribution to age (%)	Surface area (µm)
Merrillite														
SA1-7a	1.69	25.8	289	15.3	171	263	0.35	0.19	3.3	4503	135	3.0	3.2	18536
SA1-9a	0.25	1.11	22.8	4.38	90.2	21.9	4.7	0.35	3.2	4503	1307	29	2.0	3432
SA1-5a	4.35	47.0	697	10.8	160	535	0.19	0.25	3.9	4429	117	2.6	3.6	35974
SA1-4a	1.23	17.2	238	13.9	193	170	0.17	0.22	4.1	4298	161	3.8	4.0	11132
SA2-3a	0.74	5.17	78.5	7.02	107	67.9	3.0	0.33	3.3	4223	308	7.3	2.9	3443
SA2-7a	1.70	18.3	204	10.8	120	166	0.08		3.2	3842	119	3.1	3.2	9789
SB1-11a	2.81	21.8	254	7.77	90.6	199	0.25		3.0	3508	99	2.8	3.0	17734
SB1-5a	4.54	29.2	395	6.42	87.0	275	0.00		3.2	3358	94	2.8	3.3	217
SA2-2a	0.76	9.84	53.4	13.0	70.4	56.1	1.83		1.8	2805	115	4.1	1.8	4121
SB1-1b	2.88	8.39	116	2.91	40.4	76.8	0.36		2.4	2349	77	3.3	2.4	5502
SB2-1a	4.37	7.01	56.6	1.60	12.9	53.6	3.1		1.0	1442	44	3.1	1.0	10669
SB1-12a	2.59	3.28	33.7	1.27	13.0	21.7	0.95		1.1	1072	42	3.9	1.1	3655
SA2-8a	2.76	4.48	12.0	1.62	4.34	22.3	4.4		0.3	954	35	3.7	0.4	6327
SA1-9b	46.8	201	233	4.31	4.98	174	3.6		0.3	321	6.2	1.9	0.3	7211
Chlorapatite														
SB2-5a	5.10	44.4	354	8.71	69.4	505	0.56	0.10	2.0	4218	119	2.8	1.8	6182
SB2-4a	39.6	50.4	30.4	1.27	0.77	2057	0.00	0.19	0.04	4218	150	3.6	0.0	26836
SA2-9a	109	118	72.5	1.08	0.67	5315	0.01	0.21	0.04	4135	145	3.5	0.0	51677
SB1-1a	30.8	28.1	16.5	0.911	0.54	1385	0.01	0.22	0.03	4013	144	3.6	0.0	10949
SB1-4a	10.6	10.4	5.75	0.979	0.54	411	0.20		0.03	3688	131	3.6	0.0	7256

(Shuster et al., 2004). Fragments of pure chlorapatite (approximate grain radius = 43 μm) and merrillite (approximate grain radius = 59 μm) without attached phases were separated from a piece of the Guareña meteorite. Small populations of each phase (number of grains < 30) were packaged into Sn foil and exposed to a flux of ~5 × 10^{15} protons/cm^2 with incident energy ~220 MeV over a 7 h period at The Francis H. Burr Proton Therapy Center, Boston, USA. Fragments of each phase with approximately spherical geometry were then selected and dimensions were measured using a calibrated binocular microscope. One fragment of each phase was then sequentially heated in multiple steps under ultra-high vacuum while in direct contact with a thermocouple using a feedback-controlled 70 W diode laser at the BGC Noble Gas Thermochronometry Lab. The molar abundance of ^{3}He and ^{4}He was measured after each heating step using calibrated pulse-counting, sector-field mass spectrometry. Each measurement was corrected for blank contributions to ^{3}He and ^{4}He; heating schedules of each experiment are shown in Tables 2 and 3.

3. RESULTS

3.1. Single-grain (U–Th)/He data

zThe Th/U values are 7.4 ± 5.0 (average ± standard deviation) and 2.7 ± 3.5 for merrillite and chlorapatite, respectively, being generally consistent with the results of Crozaz (1974). Also, this is consistent with the Th/U of 6.8 determined for "phosphate separates" (Göpel et al., 1994) when greater abundance of merrillite than apatite in the population is considered. The Sm/Th values are 11.0 ± 5.2 and 2.1 ± 3.3 for merrillite and chlorapatite, respectively. Because of the old ages of this meteorite, and the relatively large concentrations of Sm in merrillites, the Sm contribution to the calculated (U–Th)/He age is more significant for merrillite (2.3 ± 1.2%) than in apatite (0.4 ± 0.8%). These results imply the importance of measuring Sm contents to obtain accurate (U–Th)/He ages, particularly for old merrillite samples.

The alpha recoil-uncorrected (U–Th)/He ages of the 19 phosphate aggregates in St. Séverin range broadly from 321 ± 6 to 4503 ± 135 Ma. The distribution of these ages has a peak at ~4.3 Ga with a few sporadic young ages. The oldest nine ages define tight clustering with a weighted mean of 4284 ± 65 Ma (MSWD = 1.1), which is generally consistent with the peak of the distribution. The oldest five ages are exclusively from merrillite aggregates, yielding a weighted mean of 4412 ± 75 Ma (MSWD = 0.34). If the next oldest merrillite age (3842 ± 60 Ma; SA2-7a) is included, the weighted mean is calculated as 4249 ± 155 Ma, with a resulting MSWD of 3.5. We prefer the former estimate (4412 ± 75 Ma) as a pristine merrillite (U–Th)/He age, primarily because this estimate overlaps with the peak of the probability plot (Fig. 2).

Among the five apatite ages, four generate a weighted mean of 4152 ± 70 Ma (MSWD = 0.48), which corresponds

Table 2
Stepped heating data for Guareňa merrillite.

Step	T (°C)	(±)	t (h)	[^{3}He] ($\times 10^6$ atoms)	(±) 1σ	^{4}He/^{3}He	(±) 1σ
1	525.0	0.5	0.20	1.289	0.058	1041	49
2	525.0	0.4	0.30	0.425	0.032	1012	95
3	499.7	3.3	0.75	0.257	0.024	1161	162
4	499.7	3.3	0.75	0.257	0.024	1161	162
5	474.9	2.6	1.50	0.234	0.022	992	148
6	474.9	2.6	1.50	0.245	0.023	943	137
7	424.9	2.4	2.00	0.062	0.009	643	344
8	459.8	6.9	2.00	0.170	0.018	923	181
9	509.6	9.7	1.00	0.332	0.028	1061	123
10	529.6	4.0	0.50	0.329	0.028	1017	117
11	539.6	1.1	0.50	0.329	0.028	1138	130
12	539.7	3.7	0.60	0.327	0.027	1138	128
13	549.7	3.7	0.60	0.354	0.029	1234	131
14	559.6	4.2	0.50	0.306	0.026	1230	144
15	559.7	3.8	0.60	0.417	0.032	1033	101
16	569.7	3.8	0.60	0.445	0.033	1132	103
17	579.7	3.8	0.60	0.496	0.035	1157	101
18	589.7	3.9	0.60	0.390	0.030	1434	141
19	599.4	4.0	0.60	0.427	0.032	1487	136
20	619.6	4.4	0.50	0.539	0.036	1368	109
21	639.7	4.1	0.60	0.814	0.046	1347	83
22	700.0	0.4	0.50	1.586	0.065	1424	58
23	800.0	0.4	0.50	3.185	0.093	1645	45
24	899.5	2.0	0.50	0.821	0.046	1872	110
25	1000.0	0.3	0.50	0.017	0.003	2834	3835
26	1099.9	0.5	0.50	b.d.		b.d.	

Cross dimension ~59 μm.
Measurement precision includes uncertainty in blank corrections.
b.d. is below detection limit.

Table 3
Stepped heating data for Guareña chlorapatite.

Step	T (°C)	($\pm$)	t (h)	[^{3}He] (10^6 atoms)	($\pm$) 1σ	^{4}He/^{3}He	($\pm$)
1	329.3	4.7	0.20	0.710	0.042	6774	430
2	329.5	3.7	0.30	0.351	0.029	9489	971
3	299.9	2.0	1.00	0.228	0.022	9216	1305
4	274.9	1.3	2.00	0.111	0.014	9204	2339
5	250.0	0.3	3.00	0.076	0.011	4615	1654
6	249.9	1.2	3.00	0.070	0.010	5615	2165
7	289.9	4.4	3.00	0.294	0.026	10042	1169
8	314.9	2.5	1.00	0.175	0.019	16693	2895
9	329.9	2.2	1.00	0.328	0.028	14116	1511
10	339.8	2.7	0.75	0.223	0.022	19953	2854
11	339.7	3.1	0.62	0.224	0.022	14213	2029
12	349.7	2.9	0.50	0.169	0.018	19499	3483
13	349.8	2.7	0.60	0.181	0.019	18773	3164
14	359.7	3.2	0.47	0.244	0.023	14320	1911
15	359.7	2.8	0.56	0.222	0.022	16469	2366
16	369.7	3.7	0.45	0.262	0.024	14455	1830
17	369.7	3.2	0.54	0.221	0.022	17388	2514
18	369.8	3.2	0.65	0.257	0.024	15704	2014
19	379.7	3.6	0.53	0.237	0.023	18446	2512
20	389.7	3.1	0.46	0.229	0.022	19236	2695
21	389.8	2.9	0.60	0.275	0.025	17110	2085
22	399.8	2.9	0.59	0.239	0.023	21648	2936
23	499.7	3.3	0.50	1.048	0.052	19536	968
24	599.8	2.1	0.50	0.045	0.007	42662	24186
25	700.0	0.4	0.50	b.d		b.d.	

Cross dimension ∼43 μm.
Measurement precision includes uncertainty in blank corrections.
b.d. is below detection limit.

to the peak of the probability plot (Fig. 2). With the next oldest apatite age (3688 ± 131 Ma; SB1-4a), the weighted mean becomes 4052 ± 140 Ma (MSWD = 2.8). Similarly to the merrillite, the weighted mean of four oldest ages (4152 ± 70 Ma) is expected to represent the pristine apatite (U–Th)/He age. All of the young and scattered ages are from small phosphate samples, which are more sensitive to diffusive He loss. Details of the morphological effect on the (U–Th)/He ages are discussed in the following section.

3.2. Helium diffusion kinetics in merrillite and chlorapatite

The results of our sequential degassing experiments used to quantify the kinetics of He diffusion in merrillite and chlorapatite are shown in Fig. 3 and Tables 2 and 3. We observe well-defined Arrhenius relationships for the diffusion of ^{3}He and ^{4}He in both merrillite and chlorapatite from the Guareña meteorite. Each phase presents a linear relationship across a broad range in temperature, although the results for ^{4}He in both phases indicate higher activation energy than ^{3}He. Because the ^{4}He in these samples is dominated by the natural abundance, it is possible that the natural distribution of ^{4}He is not spatially uniform. A non-uniform distribution would not satisfy the assumed initial condition in our calculation of diffusion coefficients (Fechtig and Kalbitzer, 1966). Furthermore, if the distribution of ^{4}He in each phase was modified by diffusion – even if only slightly – at any point in time prior to the experiment, a

resultant artifact can be anomalously high apparent activation energy. Alternatively, the naturally occurring ^{4}He may reside in different structural sites than the proton-induced ^{3}He; in which case, the ^{4}He results would more accurately quantify the kinetics of ^{4}He diffusion at past points in time. However, because the ^{3}He was produced by spallation reactions with stochastic trajectories via proton irradiation (Shuster et al., 2004), our assumption of a uniform distribution is better justified; proton-induced ^{3}He has been shown to share a common spatial distribution as radiogenic ^{4}He in interior fragments of Durango apatite (Shuster et al., 2004). For this reason, we consider our regression to the ^{3}He results shown in Fig. 3 to provide a better quantification of He kinetics in each sample, although use of the ^{4}He results would not significantly affect our interpretation of the St. Séverin dataset. Error-weighted regressions to ^{3}He results indicate the following diffusion parameters: E_a = 135.8 ± 4.8 kJ/mol and $\ln(D_o/a^2)$ = 5.83 ± 0.66 $\ln(s^{-1})$ for Guareña merrillite; and E_a = 109.3 ± 9.7 kJ/mol and $\ln(D_o/a^2)$ = 8.15 ± 1.93 $\ln(s^{-1})$ for Guareña chlorapatite. Assuming the analyzed fragments approximate the diffusion domain, $\log D_o$ was calculated as $(-1.93 \pm 0.29) \log(\text{cm}^2/\text{s})$ and $(-1.19 \pm 0.84) \log(\text{cm}^2/\text{s})$ for merrillite and chlorapatite, respectively. For comparison, error-weighted regressions to ^{4}He results indicate: E_a = 146.8 ± 4.9 kJ/mol and $\ln(D_o/a^2)$ = 6.98 ± 0.66 $\ln(s^{-1})$ for Guareña merrillite; and E_a = 138.2 ± 9.5 kJ/mol and $\ln(D_o/a^2)$ = 13.17 ± 1.89 $\ln(s^{-1})$ for Guareña chlorapatite. These diffusion experiments
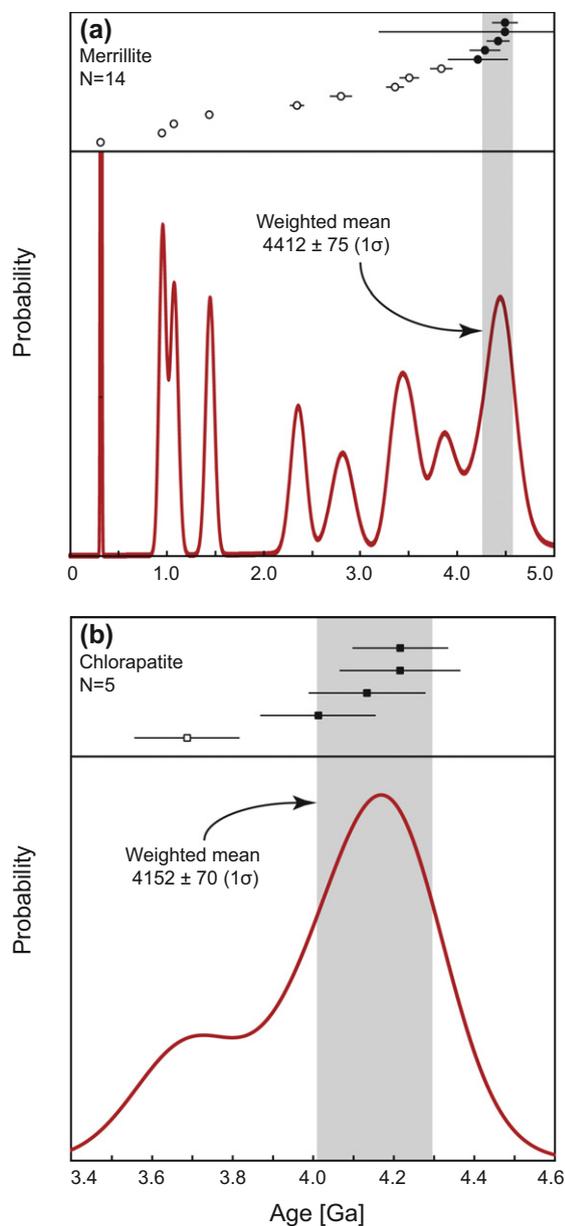
Fig. 2. Single-grain (U–Th)/He ages of phosphate aggregates from St. Séverin meteorite. (a) The weighted mean of the oldest five merrillite samples (4412 ± 75 Ma) is consistent with the peak of the probability density plot. The weighted mean age is likely to represent the timing of primary cooling as St. Séverin passed through the closure temperature of merrillite. Most of the young and scattered ages are from small phosphate samples which may have experienced partial resetting after the primary cooling. (b) Except for one outlier, four chlorapatite samples yielded concordant ages with a weighted mean (4152 ± 70 Ma) overlapping with the peak of the probability density plot. It is noteworthy that the weighted mean age of merrillites is older than that of chlorapatite, which is consistent with the relationship of closure temperatures ($T_c^{merrillite} > T_c^{Chlorapatite}$) documented from the ^{3}He and ^{4}He stepwise degassing experiments (Fig. 3). The error bars represent analytical uncertainties in 1 sigma.

clearly indicate that He is more tightly held within merrillite than it is within chlorapatite.

4. DISCUSSION

4.1. Morphology and (U–Th)/He ages

To compare morphological characteristics of phosphates, and to test if such morphological information can be used to screen good phosphate grains for (U–Th)/He dating, we examined the exposed surface of phosphates. Based on chemistry maps, we identified multiple mineral phases within each aggregate, and measured the 2-D surface areas of phosphate portions using Image-J, an image processing software.

Out of 19 aggregates used for the SEM analysis, nine aggregates contained single continuous phosphate grains, whereas the remaining ten samples exhibited multiple (up to four) phosphate islands in each aggregate. It is unclear whether each phosphate island represents an isolated phosphate grain, or they are connected below the aggregate surface, representing partial exposure of a larger phosphate grain. For our estimation, all the phosphate surface areas in the same aggregates are combined. Each of the measured phosphate surface areas is converted to a radius of a circle having the same area.

The phosphate surface areas vary from 217 μm^2 (converted radius = 8 μm) to 51,677 μm^2 (r = 128 μm), with an average of 12,665 μm^2 (r = 57 μm). The average surface area (9839 μm^2) and converted radius (51 μm) of merrillite are smaller than those of apatite (20,580 μm^2, 74 μm). Most of the phosphates have radii larger than ∼30 μm, which is larger than the natural physical dimensions of phosphates reported by Jones and Dreeland (2010). This discrepancy likely originates from our preference in selecting large phosphates during our sample screening procedure.

Assuming a spherical morphology of the natural phosphate grains, there are at least three different morphological relationships between the original phosphates and the extracted phosphate aggregates that were used for (U–Th)/He dating: (1) less than half of the original phosphate is included in the phosphate aggregate (Fig. 4a), (2) more than half of the original phosphate is included in the aggregate (Fig. 4b) or (3) the final extract is from the inner part of the original phosphate grain (Fig. 4c). Because the three possible relationships would present the same surface area of the final phosphate aggregates, it is difficult to determine to which categories the observed surface phosphates correspond. One way to test the hypothetical relationship is using U–Th–Sm contents of individual grains because the case 1 grains would yield lower U–Th–Sm abundances compared to the case 2 grains if the U–Th–Sm are homogeneously distributed in phosphates. The measured surface area and the total U–Th–Sm content were plotted in Fig. 5a. There is a general positive correlation between the age and the total U–Th–Sm content for phosphate aggregates. The two different trends are clearly demonstrated because of higher U–Th–Sm concentrations in merrillite than in apatite. The outliers can be explained either by distinctive U–Th–Sm concentrations in these samples, or different morphological categories for others. The strong positive relationship suggests that, in spite of the potential morphologic complications described above, the 2-D
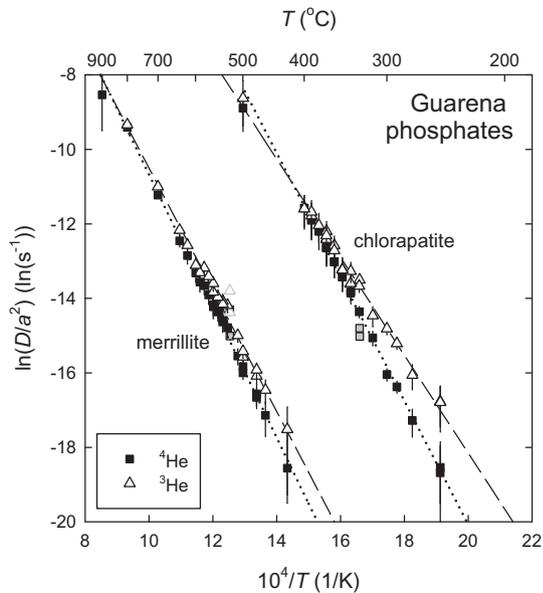
Fig. 3. Kinetics of He diffusion in merrillite and chlorapatite from the Guareña meteorite fall. Data points represent values of diffusivity (D) normalized to the square of a characteristic diffusive length-scale (a) calculated from measured release fractions of ^{3}He (triangles) and ^{4}He (squares) released during sequential stepwise degassing experiments (Fechtig and Kalbitzer, 1966), shown plotted against the absolute temperature (T) of each extraction. The experiments were conducted on single fragments of each phase (Tables 2 and 3). Lines represent error-weighted regressions through the ^{3}He (dashed) and ^{4}He (dotted) results for each phase and quantify a function $D(T)/a^2$ (i.e., an Arrhenius relationship). To minimize the influence of potential artifacts associated with surface effects, the first two steps shown in grey were excluded from each regression. In each phase the ^{3}He abundance was dominated by ^{3}He generated via laboratory proton irradiation (see text), whereas the ^{4}He was primarily natural (radiogenic or cosmogenic). Because the proton-induced ^{3}He is more likely to have a uniform spatial distribution at the beginning of each experiment, we consider the regressions to ^{3}He data to more accurately quantify the kinetics of He diffusion in these samples.

surface area represents, at least in a semi-quantitative way, an index that is proportional to the volume of the phosphate grain.

Fig. 5b illustrates the relationship between the measured 2-D surface area and (U–Th)/He ages obtained from each phosphate aggregate. The phosphate samples with large surface areas ($>\sim15,000$ μm^2) yield tightly clustered ages near ~3.5–4.5 Ga, whereas the ages from smaller samples are widely scattered in the range of 0.3–4.5 Ga. The inverse relationship between the surface area and age scatter was also detected for the ALH84001 Martian meteorite, and the relationship was explained by different scales in sampling diffusion domains (Min and Reiners, 2007). Because the samples with larger surface areas are likely to represent significant portions of their large parent phosphate crystals, they are expected to yield more consistent (U–Th)/He ages at the given thermal history. In contrast, the smaller samples may represent only small portions randomly collected from their parent phosphates, therefore they can be from anywhere between the core (yielding older ages due to diffusive gradient of He) and rim (yielding younger ages), producing relatively scattered age distribution.

Another important observation is that the average age of large samples is older than the smaller samples. This positive relationship between the size and age can be explained in that the phosphate samples with large surface areas are likely from large original grains, which have experienced relatively minor diffusive He loss compared to smaller grains. The smaller samples are most likely from smaller parent grains or from the margins of large original grains, both of which are more sensitive to diffusive He loss than larger samples. In contrast, the ALH84001 phosphates yielded almost identical average ages regardless of the sample size, although the ages for the larger grains are more scattered than for the smaller ones. This is likely due to the multiple fractures developed in the shocked meteorite of ALH84001, which generate small diffusion domains some of which can even be included within the small phosphate samples. For both shocked (e.g., ALH84001) and
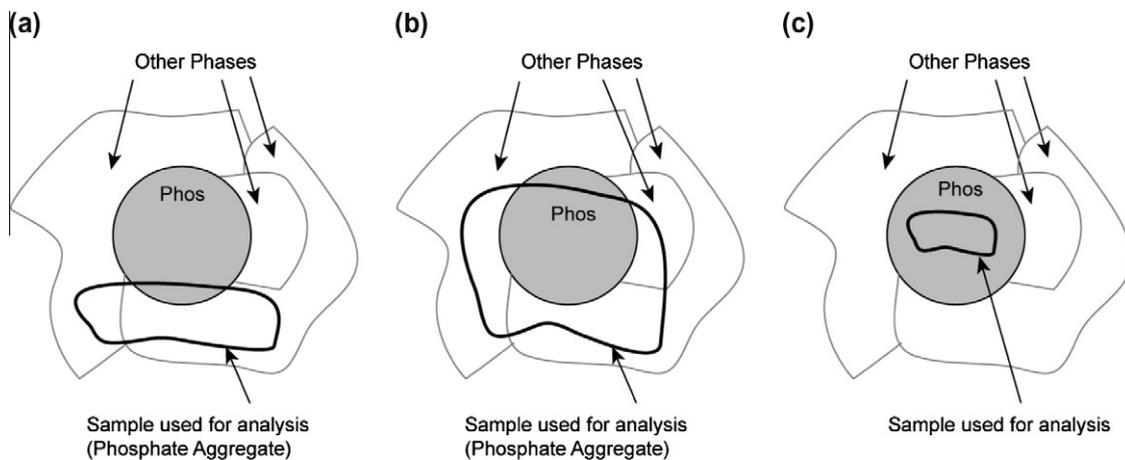

Fig. 4. Three possible explanations of the phosphate aggregates in the original meteorite. (a) The final phosphate aggregate is composed of phosphate and attached phases, and the phosphate corresponds to a small fraction (less than half) of the original phosphate volume, (b) it corresponds to a large fraction (more than half) of the original phosphate in such aggregate or (c) the final extract is almost entirely composed of phosphate, and it is from the inner part of the originally large phosphate crystal. It is difficult to distinguish (a) and (b) from 2-D morphologies described using SEM.
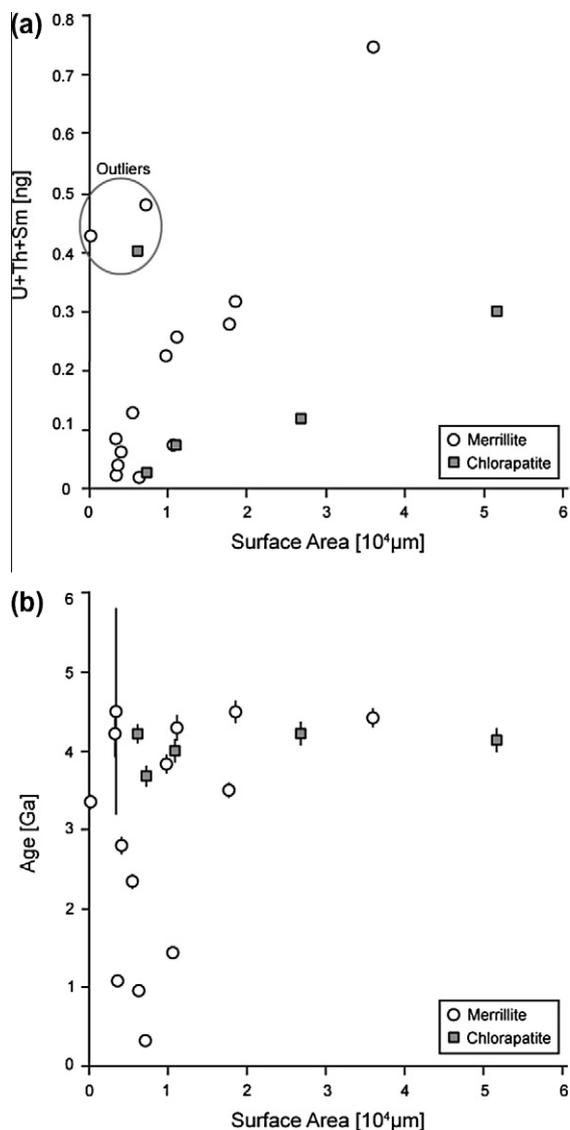
Fig. 5. Combined U–Th–Sm abundance and (U–Th)/He age against phosphate surface area. (a) Two linear trends identified for merrillite and chlorapatite suggest that the 2-D surface area of phosphate is proportional to, at least a semi-quantitative way, the volume of the phosphate grain. Systematically higher U–Th–Sm concentrations in merrillite than in chlorapatite are clearly shown. The three outliers are either from unusually higher U–Th–Sm concentrations or from different sampling of the parent phosphates as illustrated in Fig. 4b. (b) The phosphate samples with large surface areas yield tightly clustered (U–Th)/He ages, and vice versa. The inverse relationship between the surface area and age scatter likely results from the different scales in sampling diffusion domains. The phosphate samples with larger surface areas (>15,000 μm^2) yielded older ages (~3.5–4.5 Ga) because such samples are more likely from larger parent phosphate crystals.

unshocked (St. Séverin) meteorites, it is evident that large phosphate samples yield tightly clustered and reliable (U–Th)/He ages than the smaller samples. Therefore, selection of aggregates containing phosphates with large surface areas is recommended for (U–Th)/He thermochronology.

4.2. Diffusion parameters and closure temperatures

New He diffusion parameters were compared with previously reported values (summarized in Baxter, 2010). Durango fluorapatite is one of the most intensively studied terrestrial standards for (U–Th)/He thermochronology, and multiple sets of diffusion parameters were suggested: $E_a = 138.1$ kJ/mol and $D_o = 31.6$ cm^2/s from [4]He stepped heating experiments for bulk samples (Farley, 2000); $E_a = 147.87$ kJ/mol and $\ln(D_o/a^2) = 16.03$ $\ln(s^{-1})$ from proton-generated [3]He diffusion experiments (Shuster et al., 2004); $E_a = 117 \pm 6$ kJ/mol and $D_o = 0.021$ cm^2/s from [3]He implantation followed by nuclear reaction analysis (Cherniak et al., 2009). The only He diffusion data reported for meteoritic samples were obtained from two chlorapatite grains in the Acapulco meteorite: $E_a = 185.6$ kJ/mol and $\ln(D_o/a^2) = 24.1$ $\ln(s^{-1})$ (Min et al., 2003). Fig. 6 shows the calculated closure temperatures (T_c) for different diffusion parameters. The apatite closure temperatures calculated from Durango fluorapatite are generally consistent within ±5 °C for all the three pairs of diffusion parameters. The T_c of chlorapatite calculated from the Acapulco data (Min et al., 2003) is higher than for the Durango fluorapatite by ~30 °C, whereas the T_c from the new Guareña data is lower by the similar magnitude. The relatively large discrepancy in the diffusion parameters for the extraterrestrial apatites requires further investigation. The calculated T_c for merrillite is higher than any of the apatites shown in Fig. 6 suggesting the apparently sluggish He diffusion behavior in merrillite compared to terrestrial and extraterrestrial apatites. For the St. Séverin chlorapatite, we used the new data from the Guareña meteorite because both Guareña and St. Séverin (1) are chondritic in composition (H6 and LL6, respectively), (2) experienced similar thermal histories, and (3) contain the same type of apatite (chlorapatite). For merrillite, we used our experiment results from the Guareña merrillite because they are the only available data.

For the T_c calculations, it is also required to include a cooling rate at the expected T_c. Considering the general decrease of cooling rates over time revealed for many meteorite parent bodies, we estimated the maximum cooling rate at the expected T_c of merrillite (~100 °C) in St. Séverin based on the high-T cooling path defined by whole-rock Pb/Pb (Bouvier et al., 2007) and [40]Ar/[39]Ar (Hohenberg et al., 1981) data. Whole-rock [40]Ar/[39]Ar ages from a series of meteorites are used to establish thermal histories of their parent bodies (e.g., Turner et al., 1971, 1978; Pellas et al., 1997; Trieloff et al., 2003), and it is commonly assumed or proved (Renne, 2000) that those ages represent the timing of when the meteorites passed through the T_c of feldspars, which are the only K-rich phases in these meteorites. We applied the same assumption for our T_c calculations. More detailed discussions on the cooling history of St. Séverin are available in the following section.

For a diffusion domain radius of 51 μm, which corresponds to the radius converted from the average surface area of merrillite in St. Séverin (Table 1), closure temperatures of 94–112 °C were calculated for cooling rates of 0.3–2.6 °C/Ma. The upper limit of the cooling rate (2.6 °C/Ma) is inferred from the linear extension of the cooling path
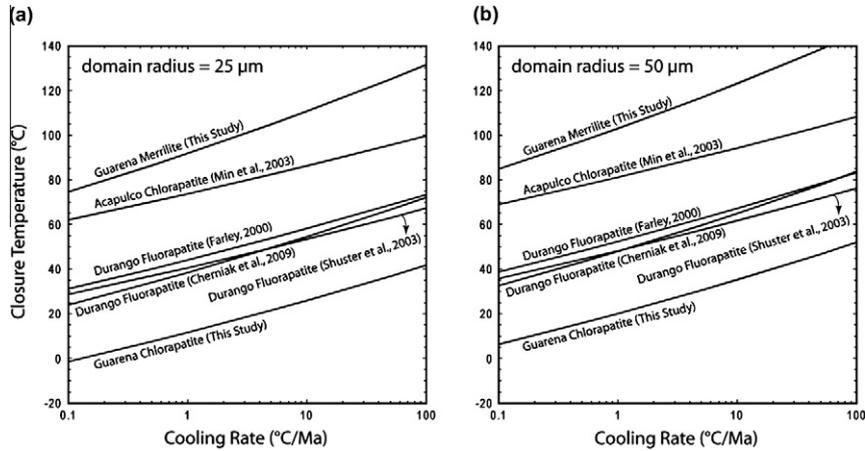
Fig. 6. Closure temperatures (T_c) of merrillite and apatite calculated for different He diffusion parameters. Two diffusion domain radii of (a) 25 μm and (b) 50 μm are used. It is unclear which diffusion parameters are more reliable, but we used the new results from the Guareña phosphates to infer the thermal history of St. Séverin because the two meteorites are both chondritic in composition and have experienced similar thermal histories. The closure temperatures are calculated as 94–112 °C and 18 °C for St. Séverin merrillite and chlorapatite, respectively.
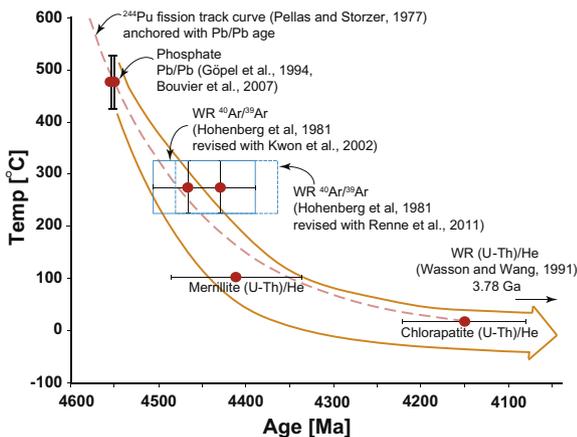

Fig. 7. Thermal history of St. Séverin inferred from all available thermochronologic data. The phosphates in St. Séverin are considered to have formed during thermal metamorphism with a maximum temperature of 900–960 °C (Huss et al., 2006), thus the phosphate Pb/Pb ages (T_c = 427–527 °C) represent the timing of cooling after the peak metamorphism. The whole-rock ^{40}Ar/^{39}Ar data (Schultz and Singer, 1976; T_c = 277 ± 20 °C) were recalculated based on updated λ–t_{FCs} pairs (Kwon et al., 2002; Renne et al., 2011). The new merrillite (U–Th)/He data suggest monotonic cooling ($\sim$2.6 °C/Ma) of St. Séverin down to $\sim$100 °C. The inferred cooling rate ($\sim$2.6 °C/Ma) is comparable with the estimates (0.9–3.8 °C/Ma) from Pu fission track data which suggested a parent body radius of 110–150 km (Pellas and Storzer, 1977, 1981).

determined from Pb/Pb and ^{40}Ar/^{39}Ar data to a low temperature range, whereas the lower limit (0.3 °C/Ma) is from the merrillite and apatite (U–Th)/He data. In consideration of apatite grains presumably having a larger diffusion domain radius of 74 μm, the closure temperatures were estimated to be $\sim$18 °C at an assumed cooling rate of 0.3 °C/Ma. The representative (U–Th)/He ages of merrillite (4413 ± 75 Ma) and apatite (4152 ± 70 Ma) show systematic variations consistent with the results obtained from the diffusion experiments ($T_c^{Merrillite} > T_c^{Chlorapatite}$).

4.3. Cooling history of St. Séverin and its implications

4.3.1. Thermochronologic constraints

The high-T thermal history of St. Séverin is mainly constrained by Pb/Pb data from whole-rock and phosphate separates. A ^{207}Pb/^{206}Pb model age of 4550 ± 10 Ma was obtained for a whole-rock sample of St. Séverin (Manhès et al., 1978). A more precise Pb/Pb model age of 4553.6 ± 0.4 Ma was obtained from a relatively small amount (1.8 mg) of phosphate separates (Göpel et al., 1994). Another approach using MC-ICP-MS yielded a reasonably consistent Pb/Pb model age of 4554.9 ± 0.1 Ma for $\sim$7 mg phosphate samples (Bouvier et al., 2007). Because the phosphates are believed to have formed during the thermal metamorphism in the parent body (Göpel et al., 1994; Dreeland and Jones, 2011), and the peak metamorphic temperature for LL6 chondrites is generally assumed to be in the range of 900–960 °C (Olsen and Bunch, 1984; Harvey et al., 1993; Huss et al., 2006), higher than Pb closure temperature in phosphates, these ages represent the period when St. Séverin passed through the Pb closure temperature of phosphate after the peak of thermal metamorphism.

The Pb diffusion in terrestrial apatite was studied by laboratory diffusion experiments (Watson et al., 1985; Cherniak et al., 1991) and empirical calibrations using geologic units of known thermal histories (Mattinson, 1978; DeWitt et al., 1984; Krogstad and Walker, 1994; Chamberlain and Bowring, 2000). These studies suggest that the Pb closure temperature of regular size apatite is in the range of 450–550 °C (Schoene and Bowring, 2006). Although Pb closure temperature of merrillite, which is the dominant phosphate in St. Séverin, is poorly understood, it is probably comparable to that of apatite, and the "phosphate closure temperature" of 427–527 °C (700–800 K) is commonly used for the mixture of merrillite and apatite in chondrites (Amelin

Table 4
Recalculated ages of Hb3gr, and dark and light samples of St. Séverin (Hohenberg et al. 1981) using various pairs of total decay constant of ^{40}K (λ) and age of Fish Canyon sanidine standard (t_{FCs}).

	t_{FCs} (Ma)	Total decay constant (10^{-10}/yr)			
		Steiger and Jäger (1977) 5.543	Kwon et al. (2002) 5.4755	Renne et al. (2010) 5.5492	Renne et al. (2011) 5.5305
Turner et al. (1971)	Not required	1072[*]			
Renne et al. (1998)	28.02	1072[*], 4383[†], 4420[‡]			
Jourdan et al. (2006)	28.02	1072[*], 4383[†], 4420[‡]			
Kwon et al. (2002)	28.269		1084[*], 4431[†], 4469[‡]		
Renne et al. (2010)	28.305			1080[*], 4397[†], 4434[‡]	
Renne et al. (2011)	28.294				1081[*], 4405[†], 4442[‡]

[*] Age of Hb3gr calculated from the most updated Ar isotopic ratio between Hb3gr and Fish Canyon sanidine (Renne et al., 2010; $R = 51.8780$).
[†] age of light sample of St. Séverin in recalculated from Hohenberg et al. (4383 Ma; 1981).
[‡] age of dark sample of St. Séverin in recalculated from Hohenberg et al. (4420 Ma; 1981).

et al., 2005; Bouvier et al., 2007). These values are also used for construction of the cooling history of St. Séverin (Fig. 7).

The medium-T thermal history is constrained by K–Ar and ^{40}Ar/^{39}Ar data. Using previously reported K concentrations (Jarosewich and Mason, 1969) combined with newly measured ^{40}Ar data, Schultz and Singer (1976) calculated a whole-rock K–Ar age of 4.40 ± 0.45 Ga. More precise and reliable estimates became available through ^{40}Ar/^{39}Ar methods. From light (1.079 g) and dark (0.993 g) rock chips of St. Séverin, Hohenberg et al. (1981) obtained ^{40}Ar/^{39}Ar age spectra with age plateaus at 4.383 ± 0.01 Ga (light) and 4.420 ± 0.01 Ga (dark) and the given uncertainties representing only analytical errors. It was noted that the systematic error from the Hb3gr flux monitor is 0.03 Ga, which should be included for absolute age determination. Therefore, the total age errors are approximately 0.04 Ga.

Because the parameters in K–Ar and ^{40}Ar/^{39}Ar dating have been updated over the past 30 years, it is necessary to recalculate the original ages based on the new parameters. The Hohenberg et al.'s (1981) ^{40}Ar/^{39}Ar ages are based on (1) the Hb3gr flux monitor with the ^{40}Ar*/K value of $5.69 \pm 0.09 \times 10^{-3}$ cm^3 STP/g specified by Turner et al. (1971), and (2) the decay constants of Steiger and Jäger (1977). Using these values, Turner et al.'s (1971) K/Ar age of Hb3gr is recalculated as 1072 ± 5.5 Ma (Renne, 2000). This age is consistent with the ^{40}Ar/^{39}Ar ages of 1073.5 ± 2 Ma (Renne, 2000) and 1073.6 ± 5.3 Ma (Jourdan et al., 2006) calibrated against the age of Fish Canyon sanidine (t_{FCs}) at 28.02 Ma. More revisions of the age of Hb3gr became necessary because of the subsequent updates of decay constants and the t_{FCs}. Table 4 shows the ^{40}Ar/^{39}Ar ages of Hb3gr calculated for different decay constants and t_{FCs} pairs using the most updated Ar isotopic ratio between Hb3gr and FCs ($R = 51.8780 \pm 0.0592$; Renne et al., 2010). Hohenberg et al.'s (1981) ^{40}Ar/^{39}Ar ages are also recalculated using the updated age of Hb3gr for different λ–t_{FCs} pairs (Table 4). Kwon et al.'s (2002) parameters ($\lambda = 5.4806 \times 10^{-10}$/yr, $t_{FCs} = 28.269$ Ma) yield revised ages of 4431.3 Ma (light) and 4468.8 Ma (dark) which are older than the original ages by ~48 Ma. If the most recently updated Renne et al.'s (2011) parameters

($\lambda = 5.5305 \times 10^{-10}$/yr, $t_{FCs} = 28.294$ Ma) are used, the ages become 4405.3 Ma (light) and 4442.4 Ma (dark) which are ~22 Ma older than the ages calculated by Hohenberg et al. (1981). It is unclear which λ–t_{FCs} pairs and sample (light or dark St. Séverin) fit better to the available thermochronologic data mainly due to (1) the large uncertainties related to the (U–Th)/He and fission track data, and (2) the poorly constrained ^{40}Ar/^{39}Ar plateaus from the two samples. Nevertheless, it is noteworthy that the ^{40}Ar/^{39}Ar age of the dark St. Séverin sample recalculated with Kwon et al.'s (2002) parameters seems to cope well with the other thermochronologic data. Because the cooling rate of the parent asteroidal body is expected to decrease over time, the older ^{40}Ar/^{39}Ar age is preferred. The ^{40}Ar/^{39}Ar data are combined with the closure temperature of 277 ± 20 °C used for H chondrites (Trieloff et al., 2003) to constrain the cooling path of St. Séverin (Fig. 7).

A cooling history was suggested for ^{244}Pu fission track densities for merrillite and adjacent silicates in St. Séverin (Pellas and Storzer, 1977a, b, revised in Pellas and Storzer, 1981). From the assumption that the fissiogenic Xe started to accumulate in merrillite at 600 ± 60 °C, a cooling rate of 3.8 °C/Ma was suggested for the temperature interval of 600–400 °C (870–670 K). Based on the fission tracks registered in merrillite and attached olivine and pyroxene crystals, Pellas and Storzer (1981) also suggested a more reliable, but significantly lower, cooling rate of 0.9 °C/Ma for a lower temperature range of ~330–30 °C. The errors of the estimated cooling rates are claimed to be ~30%. Estimated cooling rates are anchored with Pb/Pb and ^{40}Ar/^{39}Ar absolute ages and their closure temperatures (Fig. 7).

4.3.2. Cooling rates

Fig. 7 shows all of the available thermochronologic data. The whole-rock Pb/Pb and ^{40}Ar/^{39}Ar data suggest relatively rapid cooling in the temperature range of 470–277 °C at a cooling rate of 1.9 °C/Ma when Kwon et al.'s (2002) λ–t_{FCs} pair is used for ^{40}Ar/^{39}Ar age calculations. This cooling rate is lower than the previous estimate of 3.8 °C/Ma for 600–400 °C from Pu fission track data (Pellas and Storzer, 1977). However, the discrepancy can be minimized if the older ^{40}Ar/^{39}Ar ages from the dark

portion of St. Séverin are exclusively considered in combination with Kwon et al.'s (2002) parameters, which yield a high cooling rate of 3.1 °C/Ma. This cooling rate is further supported by the merrillite (U–Th)/He data because the linear extension of the cooling path down to ~100 °C (4.41 Ga) overlaps the representative (U–Th)/He age of merrillite (4.413 ± 0.075 Ga). A simple connection of Pb/Pb and (U–Th)/He data in the T-t space indicates a cooling rate of 2.6 °C/Ma which is close to the estimate from the revised ^{40}Ar/^{39}Ar ages (3.1 °C/Ma). Therefore, we conclude that St. Séverin experienced monotonic cooling from ~470 °C down to ~100 °C at a cooling rate of ~2.6 °C/Ma.

However, the estimated cooling rate is about an order of magnitude lower than modeled for a parent body of 40 km in radius (Bouvier et al., 2007), suggesting a significantly larger body size for St. Séverin. The comparison with H chondrites can also provide clues to the parent body size. The cooling paths determined for various types of H chondrites resulted in body radius estimates of 50–70 km (Pellas and Storzer, 1981), 85 km (Miyamoto et al., 1981), 55–90 km (McSween et al., 2002) and 50 km (Trieloff et al., 2003). The cooling rate of the LL6 St. Séverin estimated from the new (U–Th)/He data (2.6 °C/Ma) is lower than for H6 chondrites (~4–6 °C/Ma; Trieloff et al., 2003, revised with the decay constants of Kwon et al. (2002) and Renne et al. (2011)) in a similar temperature range of 447–117 °C, indicating that the parent body of the LL chondrites was probably larger than that of the H chondrites (Pellas and Storzer, 1981; Göpel et al., 1994; Bouvier et al., 2007).

Assuming monotonic cooling in a ~100 °C ($T_c^{Merrillite}$)–18 °C ($T_c^{Merrillite} > T_c^{Chlorapatite}$) interval, a cooling rate of ~0.3 °C/Ma is estimated from the new (U–Th)/He data. Although this cooling rate is slightly lower than expected from the Pu fission track data for the same temperature range, the entire cooling curve of our study is generally consistent with Pellas and Storzer's (1977) suggestion (Fig. 7).

4.4. Implications to alpha (α) recoil correction

The extent of α-recoil loss from the phosphate aggregates used for this study can be evaluated through a comparison with the whole-rock (U–Th)/He ages. Because the whole-rock data do not require α-recoil correction, they represent reliable overall (U–Th)/He ages. There are two reported whole-rock ages of 3.60 ± 0.45 Ga (Schultz and Singer, 1976) and 3.78 ± 0.51 Ga (Wasson and Wang, 1991). To compare these whole-rock ages with an equivalent age from the new single-grain (U–Th)/He data, we calculated a phosphate "overall age" from the abundances of U, Th, Sm and ^{4}He. Based on the total U (0.273 ng), Th (0.651 ng), Sm (3.16 ng) and He (11.8 pmol) abundances taken and combined from all of the 19 samples, a phosphate overall age of 3.53 Ga is calculated using the standard (U–Th)/He age equation. The overall age is generally consistent with the whole-rock ages of 3.60 ± 0.45 Ga (Schultz and Singer, 1976) or 3.78 ± 0.51 Ga (Wasson and Wang, 1991), within their uncertainties. The good match between the whole-rock and the overall age implies that the α-recoil loss from the phosphate samples is likely to be small. Also,

these results suggest that the phosphates are the major reservoirs of U–Th in St. Séverin. Although further quantitative estimation of the alpha recoil loss based on this approach is hampered by the large uncertainties assigned to the whole-rock ages, this provides first order confirmation that α-recoil effect is unnecessary for most of the samples selected for our (U–Th)/He dating. It is noteworthy that, although the calculated overall age is identical to the whole-rock ages, the single-grain method provides age distribution that allows for screening to determine pristine ages.

Another way to evaluate the extent of α-recoil loss from the phosphate aggregates is based on thermochronologic data. As shown in Fig. 7, the selected α-recoil-uncorrected (U–Th)/He ages are consistent with the Pb/Pb and revised ^{40}Ar/^{39}Ar ages. As previously noted, a linear extension of the cooling path determined for Pb/Pb data and an old ^{40}Ar/^{39}Ar age calculated with Kwon et al.'s (2002) parameters yields an age of 4.41 Ga at T_c of merrillite (~100 °C), which is consistent with the merrillite (U–Th)/He age. With Renne et al.'s (2011) parameters, the recalculated ^{40}Ar/^{39}Ar ages become even younger, and essentially identical to the merrillite (U–Th)/He ages. Therefore, any α-recoil correction would yield (U–Th)/He ages that are too old to cope with thermal models for the asteroidal bodies. Based on these comparisons, we conclude that the α-recoil correction is likely to be unnecessary, or at least insignificant, for the selected (U–Th)/He ages used in the calculation of the pristine ages. It is probable that the recoiled α particles are trapped within the attached phases in the phosphate aggregates, and/or the exposed phosphate surface represents the internal fracture of originally larger phosphate crystals not requiring α-recoil correction (Min, 2005). It is noteworthy that if α-recoil correction is performed based on the morphology of the selected phosphates, the resulting (U–Th)/He ages from the five merrillite aggregates would yield a weighted mean age of 5.02 Ga, which is apparently older than the accepted age of the solar system.

5. CONCLUSIONS

1. The Th/U values of 7.4 ± 5.0 and 2.7 ± 3.5 are determined for merrillite and chlorapatite, respectively. These results are generally consistent with previous reports (Crozaz, 1974; Göpel et al., 1994). The Sm/Th value determined for merrillite (11.0 ± 5.2) is higher than for chlorapatite (2.1 ± 3.3). Therefore, the contribution of Sm to the final (U–Th)/He age is more significant for merrillite (2.3 ± 1.2%) than in apatite (0.4 ± 0.8%), suggesting that Sm measurement is critical for (U–Th)/He dating of meteoritic merrillites with old ages.

2. Aggregate samples with larger surface area (>15,000 μm^2, corresponding to a radius of ~69 μm) yielded older and more tightly clustered (U–Th)/He ages (3.5–4.5 Ga), suggesting these samples are more robust to the diffusive or recoil He loss. Therefore, it is recommended to use relatively large phosphate aggregates for single-grain (U–Th)/He thermochronology. It is also important to con-

sider the natural dimensions of phosphates, then select slightly larger phosphate aggregates for (U–Th)/He dating in order to improve the chances to identify originally larger phosphate grains.

3. The oldest five (U–Th)/He ages obtained from merrillite aggregates yielded a weighted mean age of 4413 ± 75 Ma (MSWD = 0.34), whereas four apatite samples generated a weighted mean of 4152 ± 70 Ma (MSWD = 0.48). These ages correspond to the peaks of the probability density plots, and we suggest they represent the most pristine (U–Th)/He ages.

4. The proton-induced ^{3}He diffusion experiments on Guareña merrillite and chlorapatite resulted in well-defined linear trends in Arrhenius plot, yielding following diffusion parameters: $Ea = 135.8 \pm 4.8$ kJ/mol, and $\ln(D_o/a^2) = 5.83 \pm 0.66$ $\ln(s^{-1})$ for merrillite; and $Ea = 109.3 \pm 9.7$ kJ/mol, and $\ln(D_o/a^2) = 8.15 \pm 1.93$ $\ln(s^{-1})$ for chlorapatite. Assuming the analyzed fragments of merrillite (radius = 59 μm) and chlorapatite (43 μm) approximate the diffusion domain, $\log D_o$ was calculated as (-1.93 ± 0.29) log(cm^2/s) and (-1.19 ± 0.84) log(cm^2/s) for merrillite and chlorapatite, respectively. These results indicate higher closure temperature for merrillite than chlorapatite.

5. The new merrillite (U–Th)/He data combined with Pb/Pb and recalculated ^{40}Ar/^{39}Ar ages suggest monotonic cooling from ~500 °C down to ~100 °C at a cooling rate of 2.6 °C/Ma. The inferred cooling rate is lower than for H chondrites (Trieloff et al., 2003) supporting the previous suggestions that the LL chondrites experienced slower cooling compared to H chondrites (Pellas and Storzer, 1981; Bouvier et al., 2007). The estimated cooling rate is lower than for H6 chondrites suggesting that the parent body size of LL6 St. Séverin may be larger than that of H chondrites.

6. The comparison of the whole-rock (U–Th)/He ages with the new single-grain data, as well as the thermochronologic constraints, indicate that the phosphate samples that defined pristine ages do not require significant alpha recoil correction. This is probably because the selected samples are either surrounded by other attached phases, essentially shielding the alpha recoil effect, or the exposed phosphate surfaces represent the internal fractures in originally larger phosphate grains that cause no net alpha recoil loss.

REFERENCES

Amelin Y., Ghosh A. and Rotenberg E. (2005) Unraveling the evolution of chondrite parent asteroids by precise U–Pb dating and thermal modeling. *Geochim. Cosmochim. Acta* **69**, 505–518.

Baxter E. F. (2010) Diffusion of noble gases in minerals. In *Reviews in Mineralogy and Geochemistry* (eds. Y. Zhang and D. J. Cherniak). Mineralogical Society of America Geochemical Society.

Bogard D. D. (1995) Impact ages of meteorites: A synthesis. *Meteoritics* **30**, 244–268.

Bogard D. D., Husain L. and Wright R. J. (1976) ^{40}Ar–^{39}Ar dating of collisional events in chondritite parent bodies. *J. Geophys. Res.* **81**, 5664–5678.

Bouvier A., Blichert-Toft J., Moynier F., Vervoort J. and Albarede F. (2007) Pb–Pb dating constraints on the accretion and cooling history of chondrites. *Geochim. Cosmochim. Acta* **71**, 1583–1604.

Cantelaube Y., Maurette M. and Pellas P. (1967) *Radioactive Dating and Methods of Low Level Counting*. International Atomic Energy Agency, Vienna, Austria.

Cassata W. S., Shuster D. L., Renne P. R. and Weiss B. P. (2010) Evidence for shock heating and constraints on Martian surface temperatures revealed by ^{40}Ar/^{39}Ar thermochronometry of Martian meteorites. *Geochim. Cosmochim. Acta* **74**, 6900–6920.

Chamberlain K. R. and Bowring S. A. (2000) Apatite-feldspar U–Pb thermochronometer: a reliable, mid-range (~450 °C), diffusion controlled system. *Chem. Geol.* **172**, 173–200.

Cherniak D. J., Lanford W. A. and Ryerson F. J. (1991) Lead diffusion in apatite and zircon using ion implantation and Rutherford Backscattering techniques. *Geochim. Cosmochim. Acta* **55**, 1663–1673.

Cherniak D. J., Watson E. B. and Thomas J. B. (2009) Diffusion of helium in zircon and apatite. *Chem. Geol.* **268**, 155–166.

Crozaz G. (1974) U, Th and extinct ^{244}Pu in the phosphates of the St. Severin meteorite. *Earth Planet. Sci. Lett.* **23**, 164–169.

DeWitt E., Armstrong R. L., Sutter J. F. and Zartman R. E. (1984) U–Th–Pb, Rb–Sr, and Ar–Ar mineral and whole-rock isotopic systematics in a metamorphosed granitic terrane, southeastern California. *Geol. Soc. Am. Bull.* **95**, 723–739.

Dreeland L. and Jones R. H. (2011) Origin and development of phosphate minerals in metamorphosed LL chondrites. *Lunar Planet. Sci. Conf.* **42**, #2523 (abstr.).

Englert P. and Herr W. (1978) A study on exposure ages of chondrites based on spallogenic Mn-53. *Geochim. Cosmochim. Acta* **42**, 1635–1643.

Eugster O. (1988) Cosmic-ray production rates for ^{3}He, ^{21}Ne, ^{38}Ar, ^{83}Kr, and ^{126}Xe in chondrites based on ^{81}Kr-Kr exposure ages. *Geochim. Cosmochim. Acta* **52**, 1649–1662.

Farley K. A. (2000) Helium diffusion from apatite: General behavior as illustrated by Durango fluorapatite. *J. Geophys. Res.* **105**, 2903–2914.

Fechtig H. and Kalbitzer S. (1966) The diffusion of argon in potassium bearing solids. In *Potassium–Argon Dating* (eds. O. A. Schaeffer and J. Zahringer). Springer, Heidelberg.

Fritz J., Artemieva N. and Greshake A. (2005) Ejection of Martian meteorites. *Meteorit. Planet. Sci.* **40**, 1393–1411.

Ghosh A., Weidenschilling S. J. and McSween, Jr., H. Y. (2003) Importance of the accretion process in asteroid thermal evolution: 6 Hebe as an example. *Meteorit. Planet. Sci.* **38**, 711–724.

Göpel C., Manhès G. and Allègre C. J. (1994) U–Pb systematics of phosphates from equilibrated ordinary chondrites. *Earth Planet. Sci. Lett.* **121**, 153–171.

Greenwood R. C., Schmitz B. B., Bridges J. C., Hutchison R. and Franchi I. A. (2007) Disruption of the L-chondrite parent body: New oxygen isotope evidence from Ordovician relict chromite grains. *Earth Planet. Sci. Lett.* **262**, 204–213.

Hagee B., Bernatowicz T. J., Podosek F. A., Johnson M. L. and Burnett D. S. (1990) Actinide abundances in ordinary chondrites. *Geochim. Cosmochim. Acta* **54**, 2847–2858.

Harvey R. P., Bennette M. L. and McSween Jr., H. Y. (1993) Pyroxene equilibration temperatures in metamorphosed ordinary chondrites. *Lunar Planet. Sci. Conf. XXIV*. #615–616 (abstr.).

Heck P. R., Schmitz B., Baur H., Halliday A. N. and Wieler R. (2004) Fast delivery of meteorites to Earth after a major asteroid collision. *Nature* **430**, 323–325.

Heck P. R., Schmitz B., Baur H. and Wieler R. (2008) Noble gases in fossil micrometeorites and meteorites from 470 Myr old sediments from southern Sweden, and new evidence for the L-chondrite parent body breakup event. *Meteorit. Planet. Sci.* **43**, 517–528.

Heymann D. (1967) On the origin of hypersthene chondrites: Ages and shock effects of black chondrites. *Icarus* **6**, 189–221.

Hohenberg C. M., Hudson B., Kennedy B. M. and Podosek F. A. (1981) Noble gas retention chronologies for the St. Séverin meteorite. *Geochim. Cosmochim. Acta* **45**, 535–546.

Huss G. R., Rubin A. E. and Grossman J. N. (2006) Thermal metamorphism in chondrites. In *Meteorites and the Early Solar System II* (eds. D. S. Lauretta and , Jr.H. Y. McSween). University of Arizona Press, Tucson.

Jarosewich E. and Mason B. (1969) Chemical analyses with notes on one mesosiderite and seven chondrites. *Geochim. Cosmochim. Acta* **33**, 411–416.

Joliff B. L., Hughes J. M., Freeman J. J. and Zeigler R. A. (2006) Crystal chemistry of lunar and comparison to other meteoritic and planetary suites of whitlockite and merrillite. *Am. Mineral.* **91**, 1583–1595.

Jones R. H. and Dreeland L. (2010) Phosphate minerals in the LL6 chondrite, St. Séverin. *Lunar Planet. Sci. Conf. 41*. #1972 (abstr.).

Jourdan F., Verati C. and Féraud G. (2006) Intercalibration of the Hb3gr $^{40}Ar/^{39}Ar$ dating standard. *Chem. Geol.* **231**, 177–189.

Korochantseva E. V., Trieloff M., Lorenz C. A., Buykin A. I., Ivanova M. A., Schwarz W. H., Hopp J. and Jessberger E. K. (2007) L-Chondrite asteroid breakup tied to Ordovician meteorite shower by multiple isochron $^{40}Ar–^{39}Ar$ dating. *Meteorit. Planet. Sci.* **42**, 113–130.

Krogstad E. J. and Walker R. J. (1994) High closure temperatures of the U–Pb system in large apatites from the Tin Mountain pegmatitie, Black Hills, South Dakota, USA. *Geochim. Cosmochim. Acta* **58**, 3845–3853.

Kwon J., Min K., Bickel P. J. and Renne P. R. (2002) Statistical methods for jointly estimating the decay constant of ^{40}K and the age of a dating standard. *Math. Geol.* **34**, 457–474.

Lavielle B. and Marti K. (1988) Cosmic-ray-produced Kr in St. Severin core III. *Lunar Planet. Sci. Conf.* **18**, 565–572.

Manhès G., Minster J. F. and Allègre C. J. (1978) Comparative U–Th–Pb and Rb–Sr study of the Saint Sèverin amphoterite: consequences for early solar system chronology. *Earth Planet. Sci. Lett.* **39**, 14–24.

Marti K., Shedlovsky J. P., Lindstrom R. M., Arnold J. R. and Bhandari N. G. (1969) Cosmic-ray-produced radionuclides and rare-gases near the surface of St. Severin meteorite. In *Meteorite Research* (eds. P. M. Millman and D. Reidel). Holland, Dordrecht.

Mattinson J. M. (1978) Age, origin, and thermal histories of some plutonic rocks from the Salinian Block of California. *Contrib. Miner. Petrol.* **67**, 233–245.

McSween J. H. Y., Ghosh A., Grimm R. E., Wilson L. and Young E. D. (2002) Thermal evolution models of asteroids. In *Asteroids III* (eds. W. F. J. Bottke, A. Cellino, P. Paolicchi and R. P. Binzel). University of Arizona Press, Tucson, pp. 559–571.

Min K. (2005) Low-temperature thermochronometry of meteorites. In *Reviews in Mineralogy and Geochemistry* (eds. P. W. Reiners and T. A. Ehlers). Mineralogical Society of America Geochemical Society.

Min K., Farley K. A., Renne P. R. and Marti K. (2003) Single grain (U–Th)/He ages from phosphates in Acapulco meteorite and implications for thermal history. *Earth Planet. Sci. Lett.* **209**, 323–336.

Min K. and Reiners P. W. (2007) High-temperature Mars-to-Earth transfer of meteorite ALH84001. *Earth Planet. Sci. Lett.* **260**, 72–85.

Min K., Reiners P. W., Nicolescu S. and Greenwood J. P. (2004) Age and temperature of shock metamorphism of Martian meteorite Los Angeles from (U–Th)/He thermochronometry. *Geology* **32**, 677–680.

Miyamoto M., Fujii N. and Takeda H. (1981) Ordinary chondrite parent body: An internal heating model. *Proc. Lunar Planet. Sci. Conf.* **12B**, 1145–1152.

Nishiizumi K., Regnier S. and Marti K. (1980) Cosmic ray exposure ages of chondrites, pre-irradiation and constancy of cosmic ray flux in the past. *Earth Planet. Sci. Lett.* **50**, 156–170.

Olsen E. J. and Bunch T. E. (1984) Equilibrium temperatures of the ordinary chondrites. *Geochim. Cosmochim. Acta* **48**, 1363–1365.

Pellas P., Fiéni C., Trieloff M. and Jessberger E. K. (1997) The cooling history of the Acapulco meteorite as recorded by the ^{244}Pu and $^{40}Ar–^{39}Ar$ chronometers. *Geochim. Cosmochim. Acta* **61**, 3477–3501.

Pellas P. and Storzer D. (1977) Cooling histories of stony meteorites. *Lunar Planet. Sci. Conf.* **8**, 762–764.

Pellas P. and Storzer D. (1981) ^{244}Pu fission track thermometry and its application to stony meteorites. *Proc. Roy. Soc. Lond.* **A374**, 253–270.

Podosek F. A. (1970) The abundance of ^{244}Pu in the early solar system. *Earth Planet. Sci. Lett.* **8**, 183–187.

Renne P. R. (2000) $^{40}Ar/^{39}Ar$ age of plagioclase from Acapulco meteorite and the problem of systematic errors in cosmochronology. *Earth Planet. Sci. Lett.* **175**, 13–26.

Renne P. R., Swisher C. C., Deino A. L., Karner D. B., Owens T. L. and DePaolo D. J. (1998) Intercalibration of standards, absolute ages and uncertainties in $^{40}Ar/^{39}Ar$ dating. *Chem. Geol.* **145**, 117–152.

Renne P. R., Mundil R., Balco G., Min K. and Ludwig K. R. (2010) Joint determination of ^{40}K decay constants and $^{40}Ar^*/^{40}K$ for the Fish Canyon sanidine standard, and improved accuracy for $^{40}Ar/^{39}Ar$ geochronology. *Geochim. Cosmochim. Acta* **74**, 5349–5367.

Renne P. R., Balco G., Ludwig K. R., Mundil R. and Min K. (2011) Response to the comment by W.H. Schwarz et al. on "Joint determination of 40K decay constants and $^{40}Ar^*/^{40}K$ for the Fish Canyon sanidine standard, and improved accuracy for $^{40}Ar/^{39}Ar$ geochronology" by P.R. Renne et al. (2010). *Geochim. Cosmochim. Acta* **75**, 5097–5100.

Schmitz B., Lindstrom M., Asaro F. and Tassinari M. (1996) Geochemistry of meteorite-rich marine limestone strata and fossil meteorites from the lower Ordovician at Kinnekulle, Sweden. *Earth Planet. Sci. Lett.* **145**, 31–48.

Schmitz B., Tassinari M. and Peucker-Ehrenbrink B. (2001) A rain of ordinary chondritic meteorites in the early Ordovician. *Earth Planet. Sci. Lett.* **194**, 1–15.

Schultz L. and Kruse H. (1983) *Helium, Neon, and Argon in Meteorites. A Data Compilation*. Max-Planck-Institut für Chemie, Berichte aus der Meteoritenforschung.

Schultz L. and Singer P. (1976) Depth dependence of spallogenic helium, neon, and argon in the St. Severin chondrite. *Earth Planet. Sci. Lett.* **30**, 191–199.

Schoene B. and Bowring S. A. (2006) U–Pb systematics of the McClure Mountain syenite: thermochronological constraints

on the age of the ^{40}Ar/^{39}Ar standard MMhb. *Contrib. Miner. Petrol.* **151**, 615–630.

Shuster D. L., Farley K. A., Sisterson J. M. and Burnett D. S. (2004) Quantifying the diffusion kinetics and spatial distributions of radiogenic ^{4}He in minerals containing proton-induced ^{3}He. *Earth Planet. Sci. Lett.* **217**, 19–32.

Shuster D. L. and Weiss B. P. (2005) Martian surface paleotemperatures from thermochronology of meteorites. *Science* **309**, 594–597.

Steiger R. H. and Jäger E. (1977) Subcommission on geochronology: Convention on the use of decay constants in geo- and cosmochronology. *Earth Planet. Sci. Lett.* **36**, 359–362.

Trieloff M., Jesserberger E. K., Herrwerth I., Hopp J., Fieni C., Ghelis M., Bourot-Denise M. and Pellas P. (2003) Structure and thermal history of the H-chondrite parent asteroid revealed by thermochronometry. *Nature* **422**, 502–506.

Turner G., Huneke J. C., Podosek F. A. and Wasserburg G. J. (1971) ^{40}Ar–^{39}Ar ages and cosmic ray exposure ages of Apollo 14 samples. *Earth Planet. Sci. Lett.* **12**, 19–35.

Turner G., Enright M. C. and Cadogan P. H. (1978) The early history of chondrite parent bodies inferred from ^{40}Ar–^{39}Ar ages. In *Proc. 9th Lunar and Planetary Science Conference.* pp. 989–1025.

Wasserburg G. J., Huneke J. C. and Burnett D. S. (1969) Correlation between fission tracks and fission-type xenon from an extinct radioactivity. *Phys. Rev. Lett.* **22**, 1198–1201.

Wasson J. T. and Wang S. (1991) The histories of ordinary chondrite parent bodies: U, Th–He age distributions. *Meteoritics* **26**, 161–167.

Watson E. B., Harrison T. M. and Ryerson F. J. (1985) Diffusion of Sm, Sr, and Pb in fluorapatite. *Geochim. Cosmochim. Acta* **49**, 1813–1823.

Weiss B. P., Shuster D. L. and Stewart S. T. (2002) Temperature on Mars from ^{40}Ar/^{39}Ar thermochronology of ALH84001. *Earth Planet. Sci. Lett.* **201**, 465–472.

Associate editor: Hiroko Nagahara